

Top-emitting organic light-emitting diodes with Ba/Ag/indium tin oxide cathode and built-in potential analyses in these devices

J. T. Lim, J. H. Lee, and G. Y. Yeom^{a)}

School of Advanced Materials Science and Engineering, Sungkyunkwan University, Suwon 440-746, Korea

E. H. Lee and T. W. Kim

Department of Information Display Engineering, Hongik University, Seoul 121-791, Korea

(Received 5 November 2007; accepted 7 April 2008; published 1 July 2008)

Top-emitting organic light-emitting diodes (TEOLEDs) with a thin semitransparent conducting cathode (STCC) of Ba/Ag/indium tin oxide (ITO) were fabricated and their electric/optical characteristics were investigated. At the wavelength of 520 nm, optical properties of STCC of the Ba(3 nm)/Ag(15 nm)/ITO (100 nm) structure showed the transmittance of 63% and the reflectance of 37%. The light out-coupling properties of the TEOLED, which is composed of glass/Ag(150 nm)/ITO (130 nm)/4,4',4''-tris[2-naphthylphenyl-1-phenylamino]triphenylamine (2-TNATA, 30 nm)/4,4'-bis[*N*-(1-naphthyl)-*N*-phenyl-amino]-biphenyl (18 nm)/tris(8-quinolinolato)aluminum (III) (62 nm)/Ba (x nm, $x=3, 2$, and 1 nm)/Ag(15 nm)/ITO (100 nm), was increased as the deposition thickness of Ba is increased. This driving performance of the devices could be interpreted on the base of carrier injection barrier by measuring built-in voltage as well as both the optical properties and electric properties of the cathode. The optical properties (e.g., transmittance and reflectance) and electric properties of all STCCs (Ba/Ag/ITO) used in this study were nearly equal. However, built-in voltage studied using modulated photocurrent technique was increased as the thickness of barium composing of STCC was increased. This rising of a built-in voltage means a lowering of barrier height for electron injection in the devices. © 2008 American Vacuum Society. [DOI: 10.1116/1.2924333]

I. INTRODUCTION

Organic light-emitting diode (OLED) displays have been recognized in recent years as one of the promising flat panel display technologies that are capable of meeting the demand of future information-display application and lighting. Top-emitting OLED structures coupled with a low temperature polysilicon thin film transistor backplane is one of the most important key-element techniques in active-matrix OLED displays. This is because the TEOLED cannot only provide a higher aperture ratio than the general bottom-emitting diodes but also can realize higher image quality on account of its geometrical merit allowing a high pixel resolution.^{1,2}

In TEOLEDs, semitransparent top cathodes (STCCs) play an important role in achieving good device performance. This STCC should satisfy two conflicting requirements simultaneously, i.e., high electrical conductivity and high optical transmittance, to maintain the characteristics of an intrinsic top emission. Moreover, for efficient electron injection from the cathode into the electron-injecting layer such as Alq₃ [lowest unoccupied molecular orbital (LUMO) level: 3.1 eV], alkali metal [e.g., Cs (2.1 eV), and Li (2.9 eV)] and alkaline-earth metal [e.g., Ca (2.9 eV) and Mg (3.7 eV)] with a low work function have been mainly used as an adjoining cathode layer adjacent to ETL.

Many attempts have been made to develop proper top cathodes.²⁻⁹ Particular attention has been focused on the development of new cathode systems such as semitransparent

conducting buffer layers/transparent conducting oxides (TCOs) [e.g., Ag-doped Mg/tin-doped indium oxide⁶ (ITO) and Ca/ITO (Ref. 7)], multimetal cathode systems [e.g., Ca/Ag (Ref. 8) and LiF/Al/Ag (Ref. 9)], and metal-free cathode systems [e.g., copper phthalocyanine/ITO (Ref. 3) and Li-doped 2,9-dimethyl-4,7-diphenyl-1,10-phenanthroline/ITO,² Cs-doped 4,7-diphenyl-1,10-phenanthroline/Ag (Ref. 10)]. The multimetal layers used as cathode systems have been utilized to prevent physical/chemical damages to the organic layers occurring during sputter deposition of the TCOs such as ITO in the TEOLEDs.

Among the various cathode structures, Ba/Ag cathode containing Ba with low work function (2.7 eV) has been used for an efficient electron injection layer in transitional polymer light-emitting devices.¹¹ However, the TEOLEDs employing the Ba/Ag/ITO cathode as STCC have not been reported to date. In this study, the light out-coupling properties of a TEOLEDs with Ba(x nm, $x=3, 2, 1$, and 0 nm)/Ag(15 nm)/ITO (100 nm) were investigated in addition to the optical properties of the multilayer cathode and the injection barrier characteristics derived by modulated photocurrent technique. This study would be helpful in designing optimal structure of the TEOLED.

II. EXPERIMENTAL DETAILS

A. Device fabrication

Device structure of the TEOLED was composed of glass/Ag(150 nm)/ITO (130 nm)/4,4',4''-tris(2-naphthyl-

^{a)}Electronic mail: gyyeom@skku.edu

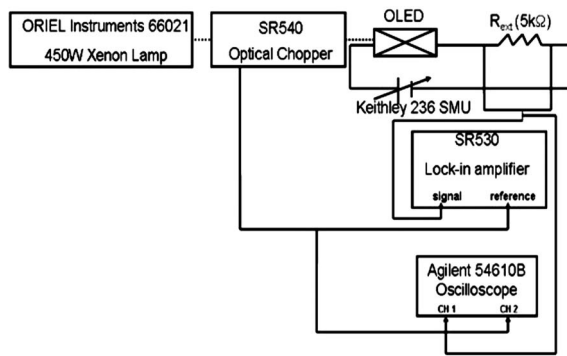


FIG. 1. Block diagram for a measurement of modulated photocurrent. The device is irradiated by the light from the xenon light source chopped by rotating blade and modulated photocurrent was measured using a lock-in amplifier and oscilloscope.

phenyl-1-phenylamino)triphenylamine (2-TNATA) (30 nm) / 4,4'-bis[*N*-(1-naphthyl)-*N*-phenyl-amino]-biphenyl (NPB) (18 nm)/Alq₃(62 nm)/Ba (x nm, $x=3, 2, 1$, and 0 nm)/Ag(15 nm)/ITO (100 nm). The Ba thickness of devices 1, 2, 3, and 4 was 3, 2, 1, and 0 nm, respectively.

A 150-nm-thick Ag layer consisting of a multilayer anode (Ag/ITO) was vacuum evaporated on a glass substrate by using a thermal evaporator. Onto this Ag layer, a 130-nm-thick ITO layer was deposited by conventional dc sputtering, followed by a heat treatment; the ITO deposition was carried out in Ar at the pressure of 5 mTorr mixed with less than 2% O₂ at the dc power of 400 W. Organic layers (2-TNATA/NPB/Alq₃) consisting of 30-nm-thick 2-TNATA as a hole-injecting layer (HIL), NPB as a hole-transporting layer, and 62-nm-thick tris(8-quinolinolato)aluminum (III) (Alq₃) as both an electron-transporting layer (ETL) and an emissive layer were sequentially deposited by using a thermal evaporator system. The x -nm-thick Ba layer and a 15-nm-thick Ag layer consisting of a multilayer cathode (Ba/Ag/ITO) were deposited onto the multiorganic layers by using a thermal evaporator. Finally, the 100-nm-thick ITO capping layer was deposited by dc sputtering in Ar at the pressure of 5 mTorr mixed with O₂ at a power of 100 W. The emissive active area of the devices was 1.4×1.4 mm².

B. Measurement of built-in voltage

The device for built-in voltage was fabricated as the glass/ITO (about 10 Ω/sq, Geomatec Co. Ltd.)/Alq₃ (150 nm)/Ba (x nm, $x=3, 2, 1$, and 0 nm)/Ag (100 nm) structure. Figure 1 shows a block diagram of an experimental setup for a measurement of modulated photocurrent. The organic light-emitting diode is connected in series with 5 kΩ external resistance, and these two devices are electrically connected to Keithley 236 source-measure unit for an application of bias voltage. The device is irradiated by the light from the 450 W xenon light source (Oriol Instruments 66021) chopped by rotating blade (Stanford Research SR540). Modulated frequency was set to 20 Hz. And modulated photocurrent generated in the diode was measured as a function of the applied bias voltage using a lock-in amplifier (Stanford Research

SR530) and oscilloscope (Agilent 54610B). Phase-sensitive lock-in amplifier measures a magnitude and phase of photocurrent.

C. General measurement

Reflectance spectra and transmittance spectra of the electrodes were measured by using a UV-visible-near infrared (UV-vis-NIR) spectrophotometer with a VW specular wavelength reflectance (Cary 5000 UV/VIS/NIR, Varian Inc.) and a UV spectrophotometer (UV S-2100, SCINCO Inc.), respectively. The resistivity was measured by using a four-point probe (CMT-SERIES, CHANG MIN Co. Ltd.). The current-voltage-luminance characteristics were measured using a source-measure unit (2400, Keithley Instrument Inc.) while the emission intensities from the TEOLED devices were measured by using the photocurrent induced on a silicon photodiode (Oriol 71608) with a picoammeter (485, Keithley Instrument Inc.). The electroluminescence (EL) spectra of the as-fabricated devices were measured by using optical emission spectroscopy (PCM-420, SC Tech. Inc.).

III. RESULTS AND DISCUSSION

In the multilayered cathode system, the use of Ba with a low work function (2.7 eV) could lead to a device performance with efficient electron injection. Meanwhile, Ag in the Ba/Ag/ITO cathode was used as a protecting layer to prevent the oxidation of both Ba and the organic layers, which are sensitive to atmospheric moisture and oxygen. A thin layer of Ag has a relatively low optical absorption and the highest conductivity among metals. In addition, ITO (refractive index: 1.95) (Ref. 12) was used as a high-refractive index-matching layer for the enhancement of the optical transmission through the top of the device and as a semipassivation layer to protect the device.

As the anode of the TEOLED, high reflectivity as a mirror and proper cavity property are required to achieve a strong radiative emission as the electric field of states is proportional to the reflectivity of the mirrors and to the reciprocal of the length of the cavity.¹² To obtain a high light-output in this TEOLED study, Ag/ITO was used as a highly reflective anode system with a good electrical conductivity, and Ba/Ag/ITO was introduced as a highly transmittable cathode system with a good conductivity.

During the deposition of ITO onto glass/Ag/ITO/organic layers/Ba/Ag, if the thickness of Ba/Ag cathode system is not thick enough, the device could be damaged by the plasma through oxidation and physical damage of the organic layers. In fact, the TEOLED with the Ag-only layer (below 12 nm in total thickness) cathode showed a poor device performance after the sputter deposition of the 100-nm-thick ITO capping layer (not shown). Therefore, the Ba(x nm)/Ag(15 nm) cathode system having the total thickness between 15 and 18 nm was used in this study, to prevent both physical damage of the organic layers and the oxidation of Ba during the ITO deposition.

Figures 2(a) and 2(b) show the transmittance curves and the reflective curves, respectively, as a function of wave-

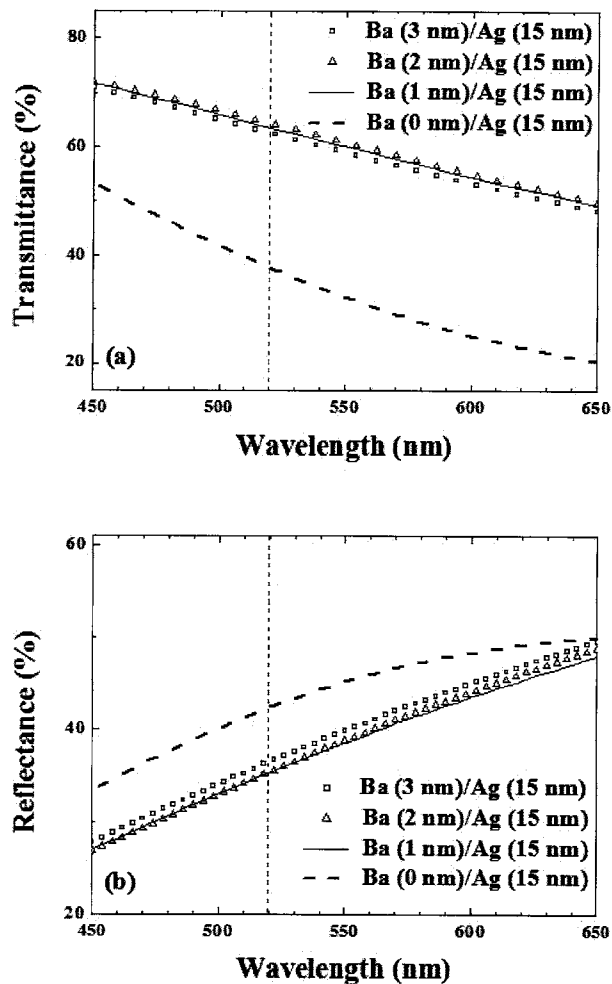


FIG. 2. (a) Transmittance spectra and (b) reflectance spectra of cathodes system composed of Ba (x nm)/Ag (15 nm)/ITO (100 nm) ($x=3, 2, 1,$ and 0 nm).

length for Ba(x nm: $x=0-3$)/Ag(15 nm)/ITO (100 nm). The transmittance of cathode was largely increased and the resistance was decreased with adding the Ba thickness in the glass/Ba(x nm)/Ag(15 nm)/ITO (100 nm) cathode, compared to cathode of Ag(15 nm)/ITO (100 nm). These optical properties are not sensitive to the change of a Ba thickness used in this study. Although the increase in transmittance with the decrease in resistance by introducing Ba into cathode is not well understood, the change of optical properties is estimated to be derived by the change of the interfacial structure between Ba and Ag.¹³

Meanwhile, cathode structure of Ba(3 nm)/Ag(15 nm)/ITO (100 nm) showed the high transmittance of 63% and the reflectance of 37% at the wavelength of 520 nm.

In addition, as shown in Table I, when the thickness of Ba in Ba(x nm)/Ag(15 nm)/ITO (100 nm) cathode is 3, 2, 1, and 0 nm, resistivities of the multilayer cathode were 5.6, 5.6, 5.7, and 5.8 Ω /sq, respectively. Also, the Ag(150 nm)/ITO (130 nm) anode showed a resistivity of about 0.2 Ω /sq.

Figure 3 shows the EL spectra of the TEOLEDs with the Ba(x nm, $x=3, 2, 1,$ and 0 nm)/Ag(15 nm)/ITO (100 nm)

TABLE I. Transmittance, reflectance, and sheet resistance of cathode system composed of Ba/Ag/ITO.

Cathode structure	Transmittance ^a (%)	Reflectance ^a (%)	Sheet resistance (Ω /sq)
Ba(3 nm)/Ag(15 nm)	63	37	5.6
Ba(2 nm)/Ag(15 nm)	64	35	5.6
Ba(1 nm)/Ag(15 nm)	64	35	5.7
Ba(0 nm)/Ag(15 nm)	38	43	5.8

^aOptical properties at the wavelength of 520 nm.

cathode and the maximum peak of the EL spectra was summarized in Table II. The maximum EL peaks of devices 1, 2, 3, and 4 were 518, 520, 520, and 520, respectively, as shown in Table II. EL spectra of the TEOLEDs are occurred from the Fabry-Pérot resonator formed by the semitransparent Ba/Ag/ITO cathode and highly reflective Ag/ITO anode, explaining the microcavity effect.¹⁴ The maximum EL peak of 520 nm was obtained by adjusting the macrocavity effect,¹⁵ which could be controlled by changing the thickness of ITO composing the multilayer anode. The EL spectrum was measured at the normal viewing angle and at L_{100} .

By using the TEOLEDs fabricated with the cathode system and the anode system described above, the current-voltage-luminance characteristics of the devices [Ba thickness in Ba/Ag(15 nm)/ITO (100 nm); devices 1, 2, 3, and 4=3, 2, 1, and 0 nm] were measured and the results are shown in Fig. 4(a). The current density-voltage-luminance characteristics and the EL characteristic for devices 1-3 were also summarized in Table II. Turn-on voltages (V_T) at the luminance of 0.1 cd/m^2 for devices 1, 2, 3, and 4 were 2.8, 2.8, 2.8, and 4.4 V, respectively. As shown in Fig. 4(a) and Table I, at a luminance of about 100 cd/m^2 (L_{100}), the current densities (J) of devices 1, 2, and 3 were 2.1 mA/cm^2

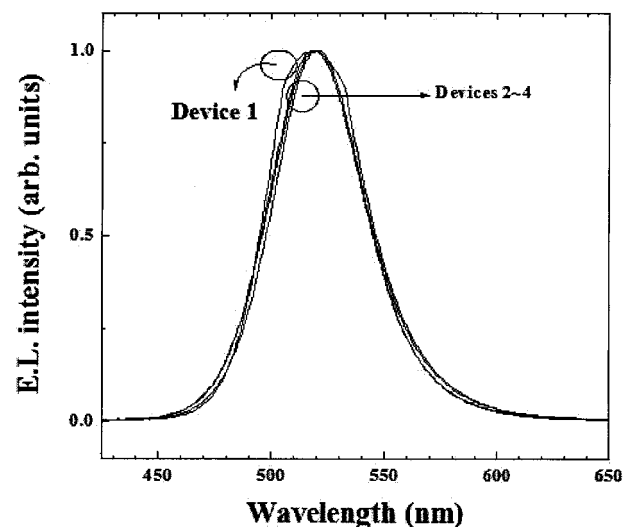


FIG. 3. Electroluminescent spectra for devices 1-4. Devices were composed of glass/Ag (150 nm)/ITO (130 nm)/2-TNATA (30 nm)/NPB (18 nm)/Alq₃ (62 nm)/Ba (x nm)/Ag (15 nm)/ITO (100 nm). (Ba thickness of devices 1, 2, 3, and 4=3, 2, 1, and 0 nm).

TABLE II. Current density–voltage–luminance characteristics and the electroluminescent properties of the devices composed of glass/Ag (100 nm)/ITO (125 nm)/2-TNATA (30 nm)/NPB (18 nm)/Alq₃ (62 nm)/BA (x nm)/Ag (15 nm)/ITO (100 nm). (Ba thickness of devices 1, 2, 3, 4, 15, 10, 5, and 0 nm).

Device	Thickness of Ba/Ag/ITO (nm)	EL λ_{\max}^a (nm)	η_L at 100 cd/m ² (lm/W)	η_{ext} at 100 cd/m ² (%)	L_{\max} (cd/m ²)	V at (100 cd/m ²) (V)
1	3/20/100	518	2.7	1.5	79 890	6.0
2	2/20/100	520	2.4	1.4	52 100	6.2
3	1/20/100	520	2.4	1.3	55 500	6.2
4	0/20/100	520	7700	10.8
					at 16.6 V	at 21.0 mA/cm ²

^aMaximum EL peaks at the luminance of 100 cd/m².

(6.0 V), 2.5 mA/cm² (6.2 V), and 2.8 mA/cm² (6.2 V), respectively. The maximum luminances (L_{\max}) for devices 1–3 were 79 890 (11.6 V), 52 100 (12.2 V), and 55 500 cd/m² (14.0 V), respectively, as shown in Table II. Figure 4(b) shows the external quantum efficiency (η_{ext}) and the power efficiency (η_{PE}) for devices 1–3 as a function of the lumi-

nance, and the results were also summarized in Table II. As shown in Fig. 4(b) and Table II, η_{PE} at L_{100} for devices 1–3 were 2.7%, 2.4%, and 2.4%, respectively, and η_{ext} at L_{100} were 1.5, 1.4, and 1.3 lm/W, respectively. When the characteristics of the devices such as V_T , J , L_{\max} , η_{ext} , and η_{PE} were compared, device 1 with the cathode structure of Ba(3 nm)/Ag(15 nm)/ITO (100 nm) showed the most excellent driving performance.

Data based on the current density–voltage–luminance characteristics exhibits that the light out-coupling efficiency is largely dependent on the thickness of Ba composing the multilayer cathode, than both the optical property and the resistivities of cathode shown Table I. This implies that the driving performance of the device is dependent on the barrier height for electron injection in the interface formed between Ba and Alq₃. Meanwhile, the carrier injection from the electrode to organic layers (ETL or HIL) of the devices could be understood by using modulated photocurrent technique.¹⁶ The built-in electric field in the device is generated by an alignment of the Fermi level of the two electrodes. The built-in voltage corresponds to a difference of work function between the anode and cathode.

A mechanism of photocurrent could be quantitatively explained. When the Alq₃ molecules absorb incident light, electrons are excited from the lower energy level to the higher one. If the applied bias voltage is zero, the excited electrons drift due to a built-in electric field. There is a photocurrent even at zero bias voltage. If the applied bias compensates a built-in voltage, excited electrons do not drift because of flatband structure. In this case, there is no photocurrent flow. When the applied bias is above the built-in voltage, there occurs an electric field across the organic layer in the opposite direction to the previous one. In this situation, the photocurrent flow direction is opposite to the previous one. This causes a phase change of photocurrent by 180°.

Figure 5(a) shows a magnitude and phase of modulated photocurrent measured using lock-in amplifier as a function of the applied bias voltage. Figure 5(a) is a result obtained from the ITO/Alq₃(150 nm)/Ba(3 nm)/Ag(100 nm) device

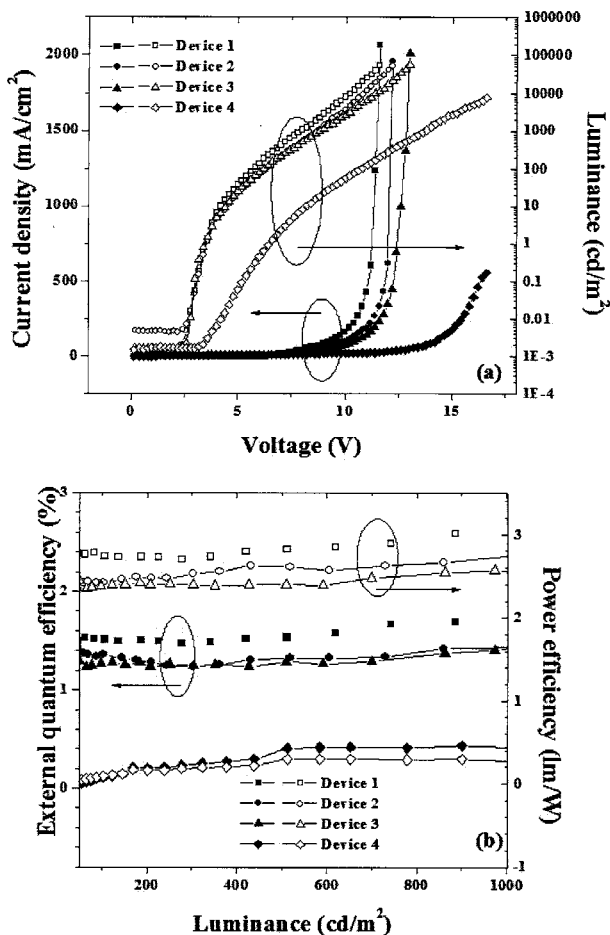


FIG. 4. (a) Current density and luminance curves as a function of bias voltage and (b) external quantum efficiency and power efficiency as a function of a luminance, for devices 1–4.

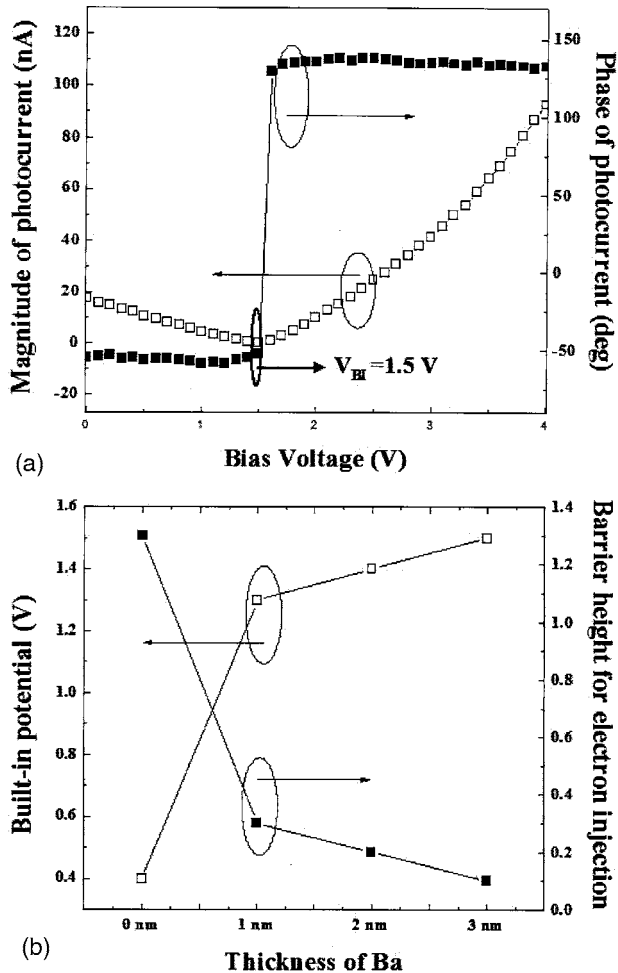


FIG. 5. (a) Magnitude and phase of modulated photocurrent measured from the device 1 of (a) ITO/Alq₃ (15 nm)/Ba (3 nm)/Ag (100 nm). (b) Built-in voltage as a function of the Ba layer thickness increases. There is an increase in built-in voltage as the Ba layer thickness increases. Open squares and solid squares represent the built-in voltage and the barrier height for electron injection, respectively, in the ITO/Alq₃ (15 nm)/Ba (*x* nm, *x* = 3, 2, 1, and 0 nm)/Ag (100 nm) device.

and Fig. 5(b) shows a built-in voltage and barrier height for an electron injection for devices 1–4. Figure 5(a) shows that as the applied bias voltage increases, the magnitude of photocurrent decreases up to certain voltage, and then increases again. In this case, the voltage when the magnitude of photocurrent is minimum is the built-in voltage ($V_{built\ in}$). Around this voltage, the phase of photocurrent changes by about 180°. In this way, when a thickness of Ba was 3 nm (device 1), 2 nm (device 2), 1 nm (device 3), and 0 nm (device 4), values of $V_{built\ in}$ were 1.5, 1.4, 1.3, and 0.4, respectively. Barrier height for electron injection (Φ_B^n) is represented by the following equation:

$$\Phi_B^n = \Phi_{anode} - E_{LUMO} - V_{built\ in}$$

Here, Φ_{anode} and E_{LUMO} correspond to work function of anode (ITO: 4.7 eV),¹⁷ energy level of the LUMO of Alq₃ (3.1 eV), respectively.¹⁸ Values of Φ_B^n for devices 1, 2, 3, and 4 were 0.1, 0.2, 0.3, and 1.3 eV, respectively. The barrier

height is dependent on the Ba/Alq₃ cathode structure used in this study and this indicates that barrier height for carrier injection is at the Alq₃/Ba interface, because the structure of the organic layers and anode was maintained same. Therefore, the light out-coupling properties in the TEOLEDs containing Ba/Ag/ITO used in this study is mainly dependent on barrier height for electron injection as well as the optical properties and the electric properties of the STCC.

IV. CONCLUSIONS

The cathode of Ba(3 nm)/Ag(15 nm)/ITO (100 nm) showed the high transmittance of 63% and a reflectance of 37%. When adding Ba to Ag(15 nm)/ITO (100 nm) cathode, the optical properties such as transmittance and a resistance was largely improved, compared to Ag(15 nm)/ITO (100 nm). Meanwhile, the light out-coupling property of the TEOLEDs with the Ba/Ag/ITO cathode system used in this study was mainly dependent on barrier height for electron injection from the Ba/Alq₃ interface into the Alq₃ layer. The device which has a structure of glass/Ag(150 nm)/ITO (130 nm)/2-TNATA (30 nm)/NPB (18 nm)/Alq₃(62 nm)/Ba(3 nm)/Ag(15 nm)/ITO (100 nm), showed the good driving performance of a high L_{max} of 79 890 cd/m² and η_{PE} of 2.7 lm/W. Also, barrier height for electron injection in the device which have the ITO/Alq₃(150 nm)/Ba(3 nm)/Ag(100 nm) structure is estimated as 0.1 eV.

ACKNOWLEDGMENT

This work was supported by National Program for Tera-level Nanodevices of the Korean Ministry of Science and Technology as one of the 21st Century Frontier Programs.

- ¹S. Miyaguchi *et al.*, Extended Abstracts Ninth International Workshop on Inorganic and Organic Electroluminescence, Bend, OR, September 1998 (unpublished), p. 137.
- ²C. Hosokawa, *Synth. Met.* **91**, 3 (1997).
- ³Z. Shen, P. E. Burrows, V. Bulovic, S. R. Forrest, and M. E. Thomson, *Science* **276**, 2009 (1997).
- ⁴H.-S. Woo, S. J. Cho, T.-W. Kwon, D.-K. Park, Y.-B. Kim, R. Czerw, D. L. Carroll, and J.-W. Park, *J. Korean Phys. Soc.* **46**, 981 (2005).
- ⁵C. W. Tang and S. A. VanSlyke, *Appl. Phys. Lett.* **51**, 913 (1987).
- ⁶P. S. Bryan, F. V. Lovecchio, and S. A. VanSlyke, U.S. Patent No. 5141671 (25 August 1992).
- ⁷F. Papadimitrakopoulos, X.-M. Zhang, D. L. Thomsen, and K. A. Higginson, *Chem. Mater.* **8**, 1363 (1996).
- ⁸R. C. Kwong *et al.*, *Appl. Phys. Lett.* **81**, 162 (2002).
- ⁹L. S. Hung, C. W. Tang, M. G. Mason, P. Raychaudhuri, and J. Madathil, *Appl. Phys. Lett.* **78**, 544 (2001).
- ¹⁰Q. Huang, K. Walzer, M. Pfeiffer, V. Lyssenko, G. He, and K. Leo, *Appl. Phys. Lett.* **88**, 113515 (2006).
- ¹¹Y. Cao, G. Yu, I. D. Parker, and A. J. Heeger, *J. Appl. Phys.* **88**, 3618 (2000).
- ¹²M.-H. Lu and J. C. Sturm, *J. Appl. Phys.* **91**, 595 (2002).
- ¹³J. W. Harris, *Handbook of Physics*, 4th ed. (Springer-Verlag, New York, 2000).
- ¹⁴S. Dirr, A. Bohler, S. Wiese, H.-H. Johannes, and W. Kowalsky, *Jpn. J. Appl. Phys., Part 1* **37**, 1457 (1998).
- ¹⁵G. Patharathy, C. Hen, A. Kahn, and S. R. Forrest, *J. Appl. Phys.* **89**, 4986 (2001).
- ¹⁶T. M. Brown and R. H. Friend, *J. Appl. Phys.* **93**, 6159 (2003).
- ¹⁷G. Partharathy, P. E. Burrows, V. Khalfin, V. G. Kozlov, and S. R. Forrest, *Appl. Phys. Lett.* **72**, 2138 (1998).
- ¹⁸M. A. Baldo and S. R. Forrest, *Phys. Rev. B* **62**, 10958 (2000).